LETTER

doi:10.1038/nature10521

Perception of sniff phase in mouse olfaction

Matthew Smear[1,2], Roman Shusterman[1], Rodney O'Connor[1]†, Thomas Bozza[1,2] & Dmitry Rinberg[1]

Olfactory systems encode odours by which neurons respond and by when they respond[1–3]. In mammals, every sniff evokes a precise, odour-specific sequence of activity across olfactory neurons[4–6]. Likewise, in a variety of neural systems, ranging from sensory periphery[7,8] to cognitive centres[9], neuronal activity is timed relative to sampling behaviour and/or internally generated oscillations. As in these neural systems, relative timing of activity may represent information in the olfactory system[10,11]. However, there is no evidence that mammalian olfactory systems read such cues[12,13]. To test whether mice perceive the timing of olfactory activation relative to the sniff cycle ('sniff phase'), we used optogenetics in gene-targeted mice to generate spatially constant, temporally controllable olfactory input. Here we show that mice can behaviourally report the sniff phase of optogenetically driven activation of olfactory sensory neurons. Furthermore, mice can discriminate between light-evoked inputs that are shifted in the sniff cycle by as little as 10 milliseconds, which is similar to the temporal precision of olfactory bulb odour responses[14,15]. Electrophysiological recordings in the olfactory bulb of awake mice show that individual cells encode the timing of photoactivation in relation to the sniff in both the timing and the amplitude of their responses. Our work provides evidence that the mammalian olfactory system can read temporal patterns, and suggests that timing of activity relative to sampling behaviour is a potent cue that may enable accurate olfactory percepts to form quickly[11,16].

If mice perceive the timing of olfactory activation, they should be able to discriminate between identical sensory stimuli presented at different times in the sniff cycle. In order to isolate this cue, we used optogenetics[17] to deliver spatially fixed, temporally controllable patterns of olfactory sensory neuron (OSN) stimulation. We engineered a mouse line in which all OSNs express channelrhodopsin-2 fused to the yellow fluorescent protein (ChR2–YFP) from the Olfactory Marker Protein (OMP) locus (Fig. 1a). In OMP–ChR2 mice, ChR2–YFP is expressed in all mature olfactory sensory neurons and their nerve terminals in glomeruli of the olfactory bulb (Fig. 1b).

To establish that we can stimulate the olfactory system with light in these mice, we first tested light detection in OMP–ChR2 ($n = 12$) and wild-type littermate controls ($n = 4$). We implanted a pressure cannula into one nasal cavity to measure sniffing, and an optical fibre in the contralateral cavity for photostimulation (Fig. 1c; see Methods). We tested these mice in a head-fixed, go/no-go task in which mice report perceptual judgments by licking or not (Fig. 1d; see Methods). We first trained mice to report odour detection. All mice achieved above-chance behavioural performance in their first session (binomial test, $P < 0.01$, 200–400 trials), and performed >90% in subsequent sessions (Fig. 1e, Supplementary Fig. 1). After at least four odour sessions, we replaced odour stimuli with light pulses (5 mW power, 1 ms duration). Under these conditions, all OMP–ChR2 mice reported detection of light with similar accuracy as for odour, within the first session (Fig. 1e), while all wild-type mice failed to report light detection above chance level in any of four sessions (binomial test, $P > 0.05$). This shows that light drives behaviour through ChR2-mediated OSN activation.

To test whether the animals perceive the sniff phase of OSN activation, we trained mice ($n = 8$) to discriminate between light stimuli solely on the basis of this cue. In each trial, a single light stimulus occurred, and across trials, stimulus intensity and duration were held constant. Stimuli were delivered 32 ms after the onset of inhalation ('go' sniff phase) or 32 ms after the onset of exhalation ('no-go' sniff phase; Fig. 2a, Supplementary Fig. 2a; see Methods). After switching

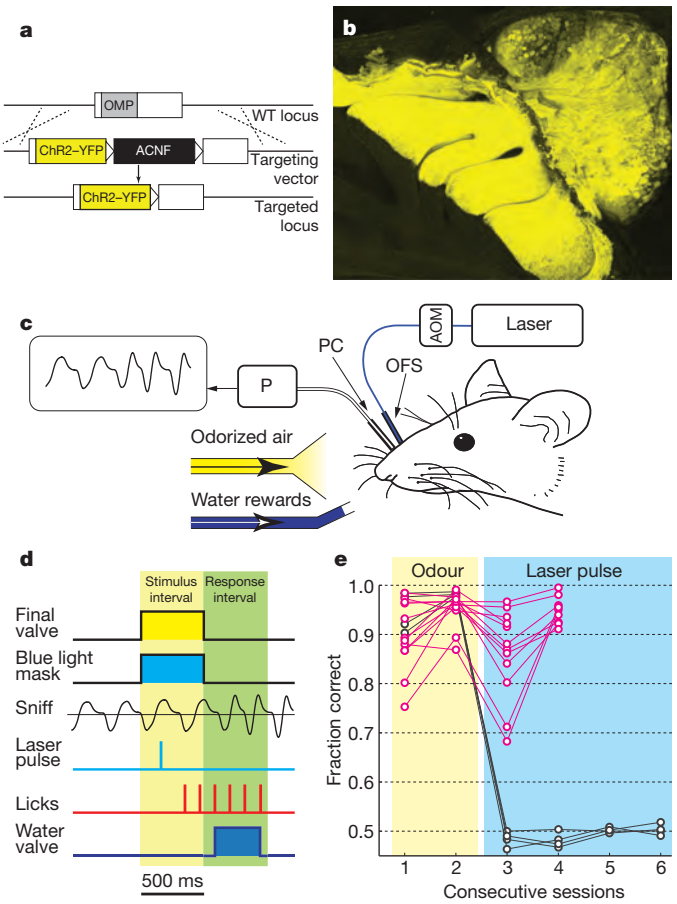

Figure 1 | Stimulating olfaction with light. **a**, Diagram of the gene targeting strategy. The ChR2–YFP sequence (yellow box) replaces that of OMP (grey box). The targeting selection cassette (ACNF) was removed by germline excision, leaving behind a single loxP site (triangle). **b**, Sagittal view of whole-mount olfactory epithelium and bulb. In OMP–ChR2 mice, ChR2–YFP labels OSNs and their axons in the bulb. **c**, Schematic of experimental set-up. Mice were implanted with a nasal optical fibre stub (OFS) to deliver light, gated by an acousto-optic modulator (AOM). A nasal pressure cannula (PC) coupled to a pressure sensor (P) measures sniffing. Inverted intranasal pressure signal is shown at top left. **d**, Behavioural trial structure. Each trial comprises a stimulus interval (yellow shading) and a response interval (green). **e**, Performance of OMP–ChR2/+ mice (pink circles; $n = 12$) and +/+ littermate controls (black circles; $n = 4$) in odour detection sessions (yellow shading), followed by light detection sessions (blue shading).

[1]Janelia Farm Research Campus, Howard Hughes Medical Institute, Ashburn, Virginia 20147, USA. [2]Department of Neurobiology, Northwestern University, Evanston, Illinois 60208, USA. †Present address: Department of Biology, Boston University, Boston, Massachusetts 02215, USA.

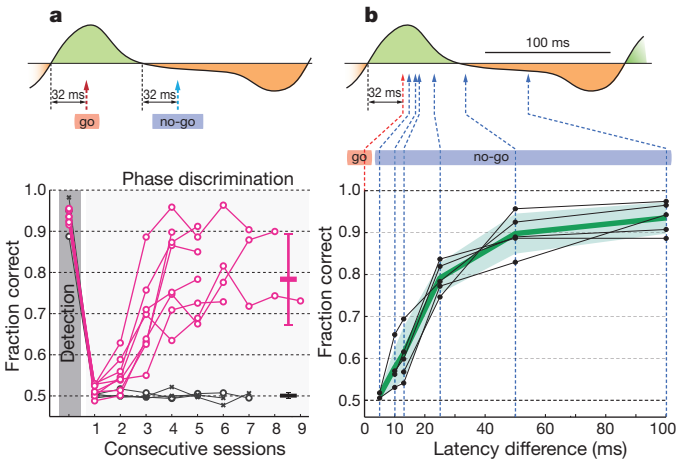

Figure 2 | OMP–ChR2 mice perceive sniff phase. **a**, Top, schematic of the sniff phase discrimination problem, shown relative to a typical sniff waveform, with inhalation shaded green and exhalation shaded orange. Light was delivered 32 ms after inhalation onset (red arrow) in 'go' trials or 32 ms after exhalation onset (blue arrow) in 'no-go' trials. Bottom, connected pink circles show the performance of OMP–ChR2/+ mice ($n = 8$) for their last light detection session, followed by phase discrimination sessions. Black lines show click detection (grey shading) and click phase discrimination performance for OMP–ChR2/+ (black circles, $n = 2$) and wild-type (black asterisks, $n = 2$). Horizontal dashes at right show mean ± s.d. phase discrimination performance for light (pink; $n = 30$ sessions) and click (black; $n = 19$ sessions) stimuli, from the third session onward. **b**, Performance as a function of latency difference. Top, as **a**. Bottom, black filled circles show performance of individual OMP–ChR2 mice while green line and shaded region give mean ± s.d. ($n = 5$).

from detection to the phase discrimination task, mice learned quickly, attaining above-chance performance in their second or third session (Fig. 2a). This behavioural performance demonstrates that mice perceive the sniff phase of olfactory input. In contrast, another set of mice ($n = 4$), tested with an easily detectable auditory click stimulus, failed to report the sniff phase of clicks (Fig. 2a, binomial test, $P > 0.05$). This suggests that the olfactory system may have unique access to sniff timing information.

How acute is the mouse's sense of time in the sniff? To test whether mice can discern finer timing differences, we trained five mice to discriminate between light stimuli occurring at the same 'go' sniff phase as above, and those occurring with varying latencies (5–100 ms) after the 'go' sniff phase (Fig. 2b, top). A single 'no-go' latency was tested in each session. Performance is high for 'no-go' latencies of 50 ms or greater (Fig. 2b). Mice maintained high accuracy at 25 ms latency (Supplementary Fig. 2b; 80 ± 5%, mean ± s.d.), and four of five mice exceeded chance performance at 10 ms (binomial test, $P < 0.01$). Achieving this performance does not require extensive training—at each latency, all mice performed three or fewer sessions. Across sessions, sniff durations do not differ systematically, but do vary from trial to trial, and mice performed better in trials with short inhalation duration (Supplementary Fig. 3). These data show that mice can sense timing differences that are tenfold shorter than a sniff cycle.

To characterize how the olfactory bulb responds to the stimuli presented in our behavioural experiments, we recorded light-evoked responses from 86 neurons, putatively mitral/tufted (M/T) cells, in the olfactory bulb of five OMP–ChR2 mice (see Methods). These mice were awake but were not performing a task. Out of 86 cells, 57% exhibited light-evoked responses: 26 gave excitatory responses, while 23 cells gave inhibitory responses (see Methods). By comparison, in a recent study, it was found that individual odours, on average, evoke responses in 66% of M/T cells[15]. Therefore, the light stimulus used in our behavioural experiments activates a similar number of M/T cells as do odours.

We then delivered light stimuli at a range of latencies relative to sniff (2–6 latencies per recording session). Some cells responded strongly at all latencies tested (for example, Fig. 3a, cell 1). In contrast, other cells exhibited varying response amplitude with stimulus latency (for example, Fig. 3a, cell 2).

To quantify the temporal dynamics of excitatory light responses, we fitted a Gaussian function to the difference between inhalation-aligned spike histograms with and without stimuli. The fit parameters yield measures of latency (τ), duration (σ) and amplitude (A) (see Methods). The brief durations (Fig. 3b) and narrow latency distribution (Fig. 3c) of these responses demonstrate that M/T cells faithfully propagate the timing of OSN photostimulation to their central targets. In addition, cells may vary their response amplitudes when stimulated at different times in the sniff cycle (for example, Fig. 3a, cell 2). Tuning curves for latency relative to sniff were heterogeneous across cells and often non-monotonic (Fig. 3c; tuning curves for cells receiving stimuli at six latencies are shown in Supplementary Fig. 4). As a result of this tuning, information about timing of OSN activation is also contained in the pattern of response amplitudes across the M/T cell ensemble. Consequently, olfactory bulb responses contain two cues that may enable the animal to report the latency of light stimuli relative to sniff onset: timing and amplitude.

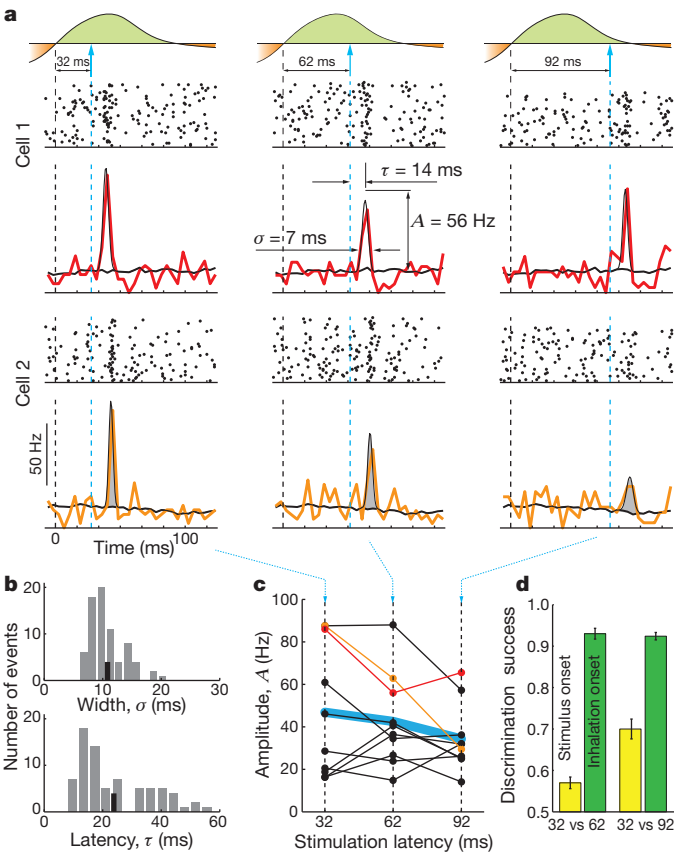

Figure 3 | Response of mitral/tufted cells to light stimulation. **a**, Top, light application. Middle and bottom, raster plots + PSTH for two cells' responses (cell 1, top; cell 2, bottom) to light at three latencies (32 ms, left; 62 ms middle; 92 ms, right) after inhalation onset. Coloured lines are PSTHs for light responses. Thick grey lines are PSTHs for spontaneous activity. Thin black line is a Gaussian fit of the difference between PSTHs for stimulated and unstimulated sniffs. The fit parameters yield measures of response width (σ), latency (τ) and amplitude (A). **b**, Distribution of response widths (σ, top) and latencies (τ, bottom). Grey bars, data; thick black line, mean. **c**, Connected filled circles show response amplitudes (A) from individual cells (red and orange dots show respectively cells 1 and 2). Blue line indicates the across-cell mean. **d**, Classification performance for the neuronal population response (mean ± s.d. across repeated permutations) discriminating between 32 and 62 ms and between 32 and 92 ms light stimulation latency. Responses were aligned to the stimulus onset (yellow) and inhalation onset (green).

We estimated the amount of information that neuronal response timing and amplitude carry about stimulus sniff-timing using a classification algorithm. In essence, this algorithm measures how well stimulus sniff phases can be discriminated on the basis of each trial's neuronal response cues (51 cells; see Methods). We compared classification success with and without the temporal cue, by applying the classification algorithm to the same neural data aligned in two ways: to inhalation onset (as in Fig. 3a), in which case both the sniff-timing and amplitude cues are available, or to stimulus onset, which eliminates the timing cue. When the classification algorithm is applied to sniff-aligned data, discrimination success for both pairs of stimuli is above 90% (Fig. 3d), comparable to behavioural performance (Fig. 2b). When applied to stimulus-aligned data, the classification algorithm performs worse, yet still above chance for both pairs of stimuli (Fig. 3d; 32 versus 62: 57 $\pm$ 1.4%; 32 versus 92: 70 $\pm$ 2.4%; see Methods). These analyses indicate that both timing and amplitude cues carry information about stimulus latency relative to sniff.

Our work provides evidence (the first, to our knowledge) that the mammalian olfactory system can read temporal information and reveals the striking temporal acuity of this mechanism. Mice discriminate between inputs solely on the basis of 'sniff phase'—that is, relative time in the sniff cycle. Whether this temporal cue is read in phase or time coordinates remains an open question[14,15]. Although mice can use timing relative to sniff in our experimental design, where this is the only cue available, it is unclear to what degree animals do so in the context of natural odour stimulation. However, the ease with which mice sense the sniff phase of olfactory input in isolation argues that this cue plays an important role in representing odours.

What mechanisms temporally pattern olfactory responses? Recent work in insects has revealed odour-specific temporal structure in OSN responses[18,19], which can largely be explained by a simple kinetic model of ligand-receptor binding[19]. Rodent OSNs also give temporally structured responses: calcium-imaging studies demonstrate odour-specific sniff-locked sequences across glomeruli[6]. These sniff-locked sequences may propagate to recipient neurons in the olfactory bulb, where additional sniff-entrained circuit mechanisms may operate. For example, M/T cells exhibit sniff-locked oscillations of membrane potential[16,20], which can transform input intensity into timing by modulating excitability[10,21]. Consistent with this idea, raising odour concentration shifts activation to earlier times in the sniff cycle[16,20]. The resultant mapping of intensity to time agrees with a theory in which latency relative to the sniff onset encodes the intensity of receptor activation[10,16,22]. Determining whether these or other mechanisms account for how the olfactory system transforms odours to sniff-locked temporal patterns will require further investigation. We provide a strong impetus for such work by showing that mice can perceive sniff phase cues.

The behavioural relevance of temporal coding has received experimental support in a variety of sensory systems[23–25]. Despite the long history of work on the temporal patterning of odour responses[4–6], the behavioural relevance of temporal coding in olfaction has not been demonstrated, despite a previous attempt to do so[12]. Our strategy of timing optogenetic activation relative to a putative timing reference signal, which has proven successful for olfaction, could be generalized to test phase/latency coding hypotheses in other systems[26]. For example, timing relative to sampling behaviour and/or local field potential oscillations has been proposed as a coding variable in vibrissal somatosensation[27] and vision[8,28]. Beyond more peripheral sensory areas, our optogenetic strategy may also be applicable to putative temporal cues in more central systems—for example, the phase precession of hippocampal place cells[9].

The ability of mice to discriminate between identical patterns of illuminated OSNs solely on the basis of timing with respect to the sniff suggests that differences in the spatial pattern of OSN activation may be unnecessary for perceptible olfactory differences, contrary to prior suggestions[13]. However, stimulus- and sniff-related signals may converge within OSNs, creating sniff-phase-dependent spatial patterns of OSN activation. In some OSNs, activity is modulated by the sniff cycle in the absence of overt odour stimulation, perhaps responding to airflow or background odour[29]. Downstream of OSNs, stimulus- and sniff-related signals may be integrated by olfactory bulb circuits, or further downstream in the olfactory system. These considerations underscore the fact that spatial coding and temporal coding are not mutually exclusive, and may instead exhibit synergy in numerous ways. We speculate that time comparisons across glomeruli give a concentration-invariant readout for odour identity[11,16,22], whereas temporal comparison to an internal representation of the sniff yields information about odour concentration. Such a coding scheme can rapidly resolve ambiguities that arise as odour identity and intensity change[11]. Extracting both parameters on a sniff-by-sniff basis may help animals locate and identify odour sources in natural olfactory scenes.

METHODS SUMMARY

OMP–ChR2 heterozygous mice and wild-type mice were implanted with headbars for head fixation, pressure cannulae in the nasal cavity for sniff recording and optic fibre stubs in the contralateral nasal cavity for light stimulus delivery. After at least three days of recovery followed by at least ten days of restriction of water intake to 1 ml d^{-1}, mice were trained to lick for water while head-fixed in a behavioural box. Then, mice were trained to perform the following behavioural tasks in a go/no-go paradigm: (1) odour detection; lick in response to odour and do not lick to blank delivery, (2) light detection; lick in response to light stimulation via nasal optic fibre (5 mW power, 1 ms duration), (3) sniff phase discrimination; lick in response to light stimulation at fixed latency after inhalation onset (32 ms) ('go' stimulus) and do not lick in response to light stimulation triggered after exhalation onset ('no-go' stimulus); and (4) fine temporal discrimination: lick in response to light stimulation at fixed latency after inhalation onset ('go' stimulus), and do not lick in response to light stimulation delayed from the 'go' stimulus latency by some time interval (5–100 ms, 'no-go' stimulus). In each session (~400 trials), one 'no-go' stimulus latency was used. Onsets of inhalation and exhalation were defined as zero-crossings of the intranasal pressure signal. For electrophysiological recordings, mice were also implanted with 16- or 32-channel silicon probes. In recording sessions, mice were awake but not performing a task. Light stimuli were triggered at fixed latencies (32, 62 and 92 ms) after onsets of inhalation or exhalation phase.

Full Methods and any associated references are available in the online version of the paper at www.nature.com/nature.

Received 26 April; accepted 2 September 2011.
Published online 12 October 2011.

1. Laurent, G. Olfactory network dynamics and the coding of multidimensional signals. *Nature Rev. Neurosci.* **3,** 884–895 (2002).
2. Friedrich, R. W. & Laurent, G. Dynamic optimization of odor representations by slow temporal patterning of mitral cell activity. *Science* **291,** 889–894 (2001).
3. Junek, S., Kludt, E., Wolf, F. & Schild, D. Olfactory coding with patterns of response latencies. *Neuron* **67,** 872–884 (2011).
4. Macrides, F. & Chorover, S. L. Olfactory bulb units: activity correlated with inhalation cycles and odor quality. *Science* **175,** 84–87 (1972).
5. Chaput, M. & Holley, A. Single unit responses of olfactory bulb neurones to odour presentation in awake rabbits. *J. Physiol. (Paris)* **76,** 551–558 (1980).
6. Spors, H., Wachowiak, M., Cohen, L. B. & Friedrich, R. W. Temporal dynamics and latency patterns of receptor neuron input to the olfactory bulb. *J. Neurosci.* **26,** 1247–1259 (2006).
7. Szabo, T. & Hagiwara, S. A latency-change mechanism involved in sensory coding of electric fish (mormyrids). *Physiol. Behav.* **2,** 331–335 (1967).
8. Gollisch, T. & Meister, M. Rapid neural coding in the retina with relative spike latencies. *Science* **319,** 1108–1111 (2008).
9. O'Keefe, J. & Recce, M. L. Phase relationship between hippocampal place units and the EEG theta rhythm. *Hippocampus* **3,** 317–330 (1993).
10. Hopfield, J. J. Pattern recognition computation using action potential timing for stimulus representation. *Nature* **376,** 33–36 (1995).
11. Schaefer, A. T. & Margrie, T. W. Spatiotemporal representations in the olfactory system. *Trends Neurosci.* **30,** 92–100 (2007).
12. Monod, B., Mouly, A. M., Vigouroux, M. & Holley, A. An investigation of some temporal aspects of olfactory coding with the model of multi-site electrical stimulation of the olfactory bulb in the rat. *Behav. Brain Res.* **33,** 51–63 (1989).
13. Leon, M. & Johnson, B. A. Is there a spacetime continuum in olfaction? *Cell. Mol. Life Sci.* **66,** 2135–2150 (2009).
14. Cury, K. M. & Uchida, N. Robust odor coding via inhalation-coupled transient activity in the mammalian olfactory bulb. *Neuron* **68,** 570–585 (2010).
15. Shusterman, R., Smear, M., Koulakov, A. & Rinberg, D. Precise olfactory responses tile the sniff cycle. *Nature Neurosci.* **14,** 1039–1044 (2011).

16. Margrie, T. W. & Schaefer, A. T. Theta oscillation coupled spike latencies yield computational vigour in a mammalian sensory system. *J. Physiol. (Lond.)* **546,** 363–374 (2003).
17. Boyden, E. S., Zhang, F., Bamberg, E., Nagel, G. & Deisseroth, K. Millisecond-timescale, genetically targeted optical control of neural activity. *Nature Neurosci.* **8,** 1263–1268 (2005).
18. Raman, B., Joseph, J., Tang, J. & Stopfer, M. Temporally diverse firing patterns in olfactory receptor neurons underlie spatiotemporal neural codes for odors. *J. Neurosci.* **30,** 1994–2006 (2010).
19. Nagel, K. I. & Wilson, R. I. Biophysical mechanisms underlying olfactory receptor neuron dynamics. *Nature Neurosci.* **14,** 208–216 (2011).
20. Cang, J. & Isaacson, J. S. In vivo whole-cell recording of odor-evoked synaptic transmission in the rat olfactory bulb. *J. Neurosci.* **23,** 4108–4116 (2003).
21. Perkel, D. H. & Bullock, T. H. Neural coding. *Neurosci. Res. Prog. Bull.* **6,** 219–349 (1968).
22. Brody, C. D. & Hopfield, J. J. Simple networks for spike-timing-based computation, with application to olfactory processing. *Neuron* **37,** 843–852 (2003).
23. Hall, C., Bell, C. & Zelick, R. Behavioral evidence of a latency code for stimulus intensity in mormyrid electric fish. *J. Comp. Physiol. A* **177,** 29–39 (1995).
24. Di Lorenzo, P. M., Leshchinskiy, S., Moroney, D. N. & Ozdoba, J. M. Making time count: functional evidence for temporal coding of taste sensation. *Behav. Neurosci.* **123,** 14–25 (2009).
25. Jacobs, A. L., Fridman, G., Douglas, R. M., Alam, N. M. & Latham, P. Ruling out and ruling in neural codes. *Proc. Natl Acad. Sci. USA* **106,** 5936–5941 (2009).
26. VanRullen, R., Guyonneau, R. & Thorpe, S. J. Spike times make sense. *Trends Neurosci.* **28,** 1–4 (2005).
27. Curtis, J. C. & Kleinfeld, D. Phase-to-rate transformations encode touch in cortical neurons of a scanning sensorimotor system. *Nature Neurosci.* **12,** 492–501 (2009).
28. Montemurro, M. A., Rasch, M. J., Murayama, Y., Logothetis, N. K. & Panzeri, S. Phase-of-firing coding of natural visual stimuli in primary visual cortex. *Curr. Biol.* **18,** 375–380 (2008).
29. Grosmaitre, X., Santarelli, L. C., Tan, J., Luo, M. & Ma, M. Dual functions of mammalian olfactory sensory neurons as odor detectors and mechanical sensors. *Nature Neurosci.* **10,** 348–354 (2007).

Supplementary Information is linked to the online version of the paper at www.nature.com/nature.

Acknowledgements We thank L. Doglio and the Transgenic and Targeted Mutagenesis Laboratory at Northwestern University for generation of chimaeric mice, B. Weiland for technical help with cloning and gene targeting, D. Huber, D. O'Connor and T. Komiyama for advice on mouse behaviour, D. Wesson and M. Wachowiak for instruction on sniff measurement, J. Nunez-Iglesias for assistance with statistics, G. Shtengel for advice on laser set-up, and T. Tabachnik and H. Davidowitz for help designing the behavioural rig. J. Osborne fabricated the microdrive. G. Lott provided digital acquisition software. A. Koulakov contributed to spike-sorting and classification algorithms. We thank W. Denk, K. Svoboda, R. Gütig, R. Egnor, M. Orger and A. Resulaj for comments on the manuscript. This work was supported by the Visiting Scientist Program at JFRC. T.B. was supported by NIDCD (R01DC009640, R21DC010911), the Whitehall Foundation and the Brain Research Foundation.

Author Contributions M.S. and D.R. designed the study and build the experimental set-up, M.S. performed the experiments and analysed the behavioural data. R.S. and M.S. performed the electrophysiological recordings, R.S. and D.R. analysed the electrophysiological data, and T.B. initiated the transgenic approach and generated the gene-targeted mice. R.O. developed the laser optics and optical fibre design. M.S., T.B. and D.R wrote the manuscript. D.R. and T.B. supervised the project.

Author Information Reprints and permissions information is available at www.nature.com/reprints. The authors declare no competing financial interests. Readers are welcome to comment on the online version of this article at www.nature.com/nature. Correspondence and requests for materials should be addressed to D.R. (rinbergd@janelia.hhmi.org) or T.B. (bozza@northwestern.edu).

METHODS

Gene targeting. The coding sequence for ChR2(H134R)–YFP (gift of G. Nagel, Max Planck Institute for Biophysics) was amplified and cloned into an OMP targeting vector[30] replacing the endogenous OMP coding sequence. The vector also contained an autoexcising *neo* selection cassette[31]. The vector was linearized and electroporated into E14 ES cells, and correctly targeted clones isolated using standard methods. Targeted clones were injected into C57BL/6J blastocysts to generate chimaeras. The allele was passed through the male germline, removing the *neo* cassette. The OMP–ChR2–YFP line was derived from clone 'OCY-58'. This strain will be made available through The Jackson Laboratory (Tyr<c-2J>-OMP<tm1(COP4/EYFP)-Tboz>/J; STOCK #14173); address requests for information to T.B.

Animals. Data were collected in 15 OMP–ChR2–YFP heterozygous mice and 4 wild-type littermates. All mice had at least one normal copy of OMP. Subjects were 6–8 weeks old at the beginning of behavioural training and were maintained on a 12 h light/dark cycle (lights on at 8:00 p.m.) in isolated cages in a temperature- and humidity-controlled animal facility. All animal care and experimental procedures were in strict accordance with a protocol approved by the Howard Hughes Medical Institute Institutional Animal Care and Use Committee.

Sniff recording. To monitor the sniff signal, a 7-mm-long stainless cannula (gauge 23, Small Parts capillary tubing) was implanted in the nasal cavity. The cannula was capped between experimental recordings. During experiments, the cannula was connected via polyethylene tubing (801000, A-M systems) to a pressure sensor (MPX5050, Freescale Semiconductor) and custom-made preamplifier circuit. The signal from the preamplifier was amplified 20× and low-pass-filtered below 20 Hz (Cygnus Technology), digitized with an NIDAQ board (National Instruments) and acquired by an in-house data acquisition program (SpikeHound, written by G. Lott). The pressure signal was also sent to a custom-made comparator board that created a square TTL pulse between rising and falling zero crossings in the pressure signal. This pulse went to a behavioural control board to trigger light stimuli (see below).

Surgery. Mice were anaesthetized using isofluorane gas anaesthesia. The horizontal bar for head fixation, pressure cannula, optic fibre stub, and, in a subset of mice, electrode chamber were implanted during a single session of surgery. To implant the sniffing cannula, a small hole was drilled in the bone overlying the nasal cavity, into which the cannula was inserted and affixed with glue and stabilized with dental cement. The optic fibre stub was implanted and fixed in the same way in the contralateral nasal cavity. To implant the electrode chamber, a small craniotomy ($\sim$1 mm^2) was opened above the olfactory bulb, roughly centred along the A–P and M–L axes of the bulb. An electrode chamber with a silicon probe was fixed by dental cement to the skull, posterior to the olfactory bulb. The reference electrode was implanted in the cerebellum. After surgery, a mouse was caged individually and given at least 3 days for recovery.

Stimulus delivery. For odour stimulus delivery, we used a nine-odour air dilution olfactometer. Odorants (Sigma-Aldrich) were stored in liquid phase in dark vials. The airflow through the selected odorant vial was diluted 10 times by the main airflow stream and homogenized in a long thin capillary before reaching the final valve. Between stimuli, a steady stream of 1,000 ml min^{-1} of clean air flowed to the odour port continuously, while the flow from the olfactometer was directed to an exhaust. During stimulus delivery, the final valve (four-way Teflon valve; NResearch) switched the odour flow to the odour port, and diverted the clean airflow to the exhaust. Temporal odour concentration profile was checked by a mini photoionization detector (miniPID, Aurora Scientific). The concentration reached a steady state 25–40 ms after final valve opening.

A 473-nm laser (Ciel Blue DPSS, Photonic Solutions) was our light source. The main beam was split to provide stimulus for two experiments. Each secondary beam was gated by an acousto-optic modulator (AOM, QuantaTech), which enabled analogue control of light stimulus power with microsecond timing precision. A fibre launcher (Thorlabs) was positioned to catch the first mode from the AOM in a 100 μm core multi-mode optic fibre. The amplitude of the square pulse controlled the angle of AOM beam diversion, thus providing fine control of power collected by the fibre launcher.

The opposite end of the fibre terminated in a ceramic ferrule (Precision Fibre Products), which could be coupled via an phosphor-bronze sleeve (Optequip) to an identical ceramic ferrule holding the optical fibre stub implanted into the mouse. The light stimulus power at the ferrule ending was measured by a power-meter (Thorlabs), and calibrated daily by adjusting the amplitude of the pulse to the AOM driver. The ferrule coupling allowed efficient transmission of light (80–90%), but also leaked light. To prevent the mouse from using this leaked light as a visual cue, two bright blue LEDs (Luxeon V-star, Philips Lumileds Lighting Company) were positioned on either side of the mouse's head, about 1 cm from each eye. These LEDs were activated during the stimulus period of each trial, to mask leak light from the laser.

Water delivery was based on gravitational flow controlled by a solenoid valve (Clippard) connected via Tygon tubing to a stainless steel cannula (gauge 21, Small Parts), which served as a lick tube. The lick tube was positioned near the animal's mouth, and could be moved by a micromanipulator. The water volume was controlled by the duration of valve opening for 200–400 ms duration, calibrated daily to give approximately 5 μl per opening. Licks were detected by photodiode beam break by the mouse's tongue.

Behavioural control. All behavioural events (odour and final valve opening, laser delivery, water delivery, and photobeam crossing) were monitored and controlled by a behavioural board (LASOM1, RPMetrix), which allowed real-time experimental control with millisecond precision. The behavioural board reads trial parameters and sends trial results to a PC running custom-written MatLab routines (Mathworks).

Behavioural task and training. After at least 3 days of post-operative recovery and at least 7 days of water restriction (1 ml d^{-1}), we began to train the mice. Training started with water-sampling sessions, in which the mouse was placed in the head fixation set-up and given water for licking. Before moving to the next stage of training, each mouse had to perform two sessions in which it licked enough to receive its full 1 ml of water for the day. Mice that failed to collect their full daily ration in a behavioural session were supplemented with water in their home cage.

Next, the mice were trained to report odour detection. A behavioural session was broken into pseudo-randomly ordered trials, each of which consisted of a stimulus period, a response period, and an intertrial interval (ITI). During the stimulus period, the final valve switched to direct air from the olfactometer to the animal. Olfactometer flow passed through a vial containing liquid odorant, or through a blank vial. Mice received water for licks during the response period following odour delivery, and did not receive water if they licked in response to blank delivery. These incorrect licks were punished by lengthened ITI. Correct trial ITIs were 5,000 ms plus a random number between 1 and 2,000 ms, while incorrect trial ITIs were 10,000 ms plus a random number between 1 and 6,000 ms. Randomization of ITIs was intended to prevent the possibility that animals would anticipate stimulus delivery and synchronize their sniffing.

After at least two sessions with a first odorant, another odour became the 'go' stimulus. In pilot experiments, we found that mice usually would not lick for a new stimulus under these conditions, but only for the initially trained odorant. In order to facilitate more rapid acquisition of licking for new stimuli, we included an 'associative block' at the beginning of every session. The associative block consisted of ten water valve openings delivered immediately after fixing the mouse in the behavioural chamber, followed by 20 consecutive 'go' trials with the new stimulus. Acquisition blocks were included in all behavioural sessions reported here.

Light sessions began after at least four odour detection sessions for each mouse. Licking in response to light stimulus was rewarded with water. Licking when no light stimulus was delivered lengthened the ITI. For all light sessions, the stimulus power at the ferrule coupling was 5 mW, while the stimulus duration was 1 ms. Pilot experiments suggested that stimuli roughly an order of magnitude more powerful or longer duration could be detected by +/+ mice. All OMP–ChR2/+ mice reported light detection. Only those mice that maintained a good sniff signal could be tested for the temporal discriminations.

After at least one session of light detection, mice began sniff phase discrimination sessions. In these, light was triggered from a rising or falling zero crossing in the sign-inverted pressure signal, which indicate the onset of inhalation or exhalation, respectively. Reliable detection of zero-crossing events was facilitated by low pass filtering sniff signals below 20 Hz, which introduced a constant delay of 32 ms, as described in the text. After at least three sniff phase discrimination sessions, those mice that maintained a good sniff signal were tested for the finer latency discriminations. In each of these sessions, a single no-go stimulus was used, and each mouse did three or fewer sessions at each latency, in descending order.

Electrophysiology. Mitral/tufted cell spiking activity was recorded using 16- or 32-channel silicon probes (NeuroNexus, models a2x2-tet-3mm-150-150-312(F16), a4x8-5mm 150-200-312(F32)). Cells were recorded in the mitral cell layer of the dorsal bulb, 300–400 μm from the bulb surface. The identity of M/T cells were established based on the criteria formulated in previous work[32]. The data were acquired using 32-channel data acquisition system (Digital Lynx, NeuraLynx) with widely open broadband filters and sampling frequency 0.1–9,000 Hz.

Data analysis and spike extraction. Data analysis was done in MatLab (Mathworks). Acquired electrophysiological data were filtered and spike sorted. For Si-probe data we used the M-Clust program (written by A. D. Redish) and a software package (written by A. Koulakov).

Light responses. To identify excitatory and inhibitory responses in neurons, we used a randomization test to compare the distributions of total spike counts of each cell with and without light stimulation[33]. In each session, 3,000–5,000 sniff cycles without light stimulation nor following light stimulation within 5 cycles were

defined as control cycles. N cycles with light stimulation (one sniff cycle per trial with stimulus) were test cycles ($N = 22$–70). For time windows of 1, 2, ... 100 ms after stimulus onset, we counted the number of spikes in the time window across the N trials. We then compared this number against the distribution of spike counts in the same time window for randomly chosen subsets of size N from the control cycles. The P value was estimated as the proportion of control spike counts larger than the observed test count, relative to the distribution median, multiplied by 2 to account for the two-sidedness of the test. We considered a cell to respond to the stimulus if the P value for at least one time window was less than 0.003, which corresponded to a false discovery rate of 0.05 by the Benjamini-Hochberg procedure. For statistically significant excitatory responses, we fitted a Gaussian, $f = A\exp[-\pi(t-\tau)^2/\sigma^2]$, to the difference between spike histograms for stimulated and unstimulated sniffs, where A is the amplitude of the response, τ is its average latency, and σ is its average width. The parameter σ is chosen so that $A \times \sigma$ is equal to the integral below the Gaussian function and corresponds to the average number of extra spikes per trial in response to the stimulus.

Classification analysis. To estimate how well a population of neurons ($n = 51$) can discriminate between two stimuli on a single trial, we used a template-matching algorithm [15]. For each pair of stimulus latencies (light stimulation at 32 and 62 ms latency, and at 32 and 92 ms latency), we aligned neuronal signals in two ways, relative to the inhalation onset or relative to the stimulus onset. For every trial we built a response vector $\mathrm{r}_k = \{r_{1,1}, r_{1,2}, \ldots r_{1,m}, r_{2,1}, \ldots r_{2,m}, \ldots r_{n,m}\}$, where individual components, $r_{i,j}$, were number of spikes in a time bin $j (j = 1, \ldots m)$ of a neuron $i (i = 1, \ldots n)$. Time bins of 10 ms covered the interval from either the onset of inhalation or stimulus for the duration of 150 ms. For every stimulus and every trial, we estimated template vectors $\mathrm{r}_{k,s} = \langle r_i \rangle_{i, i \neq k, S(i) = s}$ (where $S(i)$ is a stimulus type for a trial i, and $\langle \rangle_i$ is averaging over i), which averaged all trials for each stimuli $s = 1,2$, excluding the given trial k. Then we assigned a given trial to one of the templates based on the shortest Euclidian distance between the response vector $\mathbf{r}_k$ and the templates' vectors $\bar{\mathrm{r}}_{k,s}$. The classification success was equal to a portion of correct assignments.

30. Bozza, T., McGann, J. P., Mombaerts, P. & Wachowiak, M. In vivo imaging of neuronal activity by targeted expression of a genetically encoded probe in the mouse. *Neuron* **42,** 9–21 (2004).
31. Bunting, M., Bernstein, K. E., Greer, J. M., Capecchi, M. R. & Thomas, K. R. Targeting genes for self-excision in the germ line. *Genes Dev.* **13,** 1524–1528 (1999).
32. Rinberg, D., Koulakov, A. & Gelperin, A. Sparse odor coding in awake behaving mice. *J. Neurosci.* **26,** 8857–8865 (2006).
33. Garthwaite, P. H., Jolliffe, I. T. & Jones, B. *Statistical Inference* (Oxford Univ. Press, 2002).